15

The use of morphometric variables in the surface topography study of X-ray optical elements

© A.A. Dedkova,[1,2] I.V. Florinsky,[2] A.K. Chernyshev[3]

[1] National Research University of Electronic Technology
124498 Zelenograd, Moscow, Russia
[2] Institute of Mathematical Problems of Biology, Keldysh Institute of Applied Mathematics, Russian Academy of Sciences,
142290 Pushchino, Russia
[3] Institute of Physics of Microstructures, Russian Academy of Sciences,
607680 Nizhny Novgorod, Russia
e-mail: dedkova@ckp-miet.ru, iflor@mail.ru

Received April 13, 2023
Revised April 13, 2023
Accepted April 13, 2023

We studied the use of morphometric variables (maximal curvature, minimal curvature, mean curvature, topographic index, etc.) for study of the surface of X-ray optical elements. We performed calculations on digital elevation models of a spherical concave substrates: primordial and smoothed digital elevation models, before and after technological operations (mechanical lapping, axisymmetric surface shape correction, ion beam figuring). We have demonstrated a visual display of weakly expressed topographic inhomogeneities, incl. which are not displayed on the maps of the original digital elevation models. The consideration included the study of both the measured samples and the errors in the formation of the digital elevation model (artifacts from the recording system and from the inhomogeneity of the medium), as well as the features of scale decomposition when using the universal spectral-analytical method.

Keywords: surface, topography, digital elevation model, DEM, multilevel analysis, shaping, aspherization, interferometry, x-ray optics, multilayer interference mirror, curvature, morphometric variable, geomorphometry, defect, measurement artifact.

DOI: 10.61011/TP.2023.07.56651.89-23

Introduction

In the manufacturing of X-ray optics, much attention is paid to the control of the shape of the manufactured reflective elements. The accuracy of the shape of the manufactured surface determines the resolution of X-ray mirrors [1].

A large number of works by various scientific groups [1–8] are devoted to the formation of the surface of a given profile, or, in other words, the control of the local curvature of the surface of optical elements [1–17]. The shape correction process is iterative and requires at each stage of correction the measurement and analysis of the shape of the surface [2]. The specific required volumes of technological impact are calculated using the generated surface map, for example, the parameters of the ion beam (size, current, energy, local angle of incidence of ions on the surface, etching rate, etc.) to develop an optimal etching algorithm that allows forming the required surface shape [2].

Many hundreds of papers are devoted to issues related to approaches to the study of the topography and shape of objects. However, the direction dedicated to multilevel surface analysis (large-scale decomposition) should be singled out separately. Such a technique can be useful for selecting objects of a given size, for example, detecting the location of filler particles in the medium when processing atomic-force microscopy (AFM) data [18,19]. In the study of the digital elevation model (DEM) of the surface acquired using AFM in the paper [18] it was represented by the sum of two topographies: a slowly changing topography of low curvature (the surface of the macro level of the material) and a topography of high curvature (the surface of the nanoscale of the material) —an integral filter was used for separation. The separation of the initial topography into three components with curvature of different scales is considered also for the DEM acquired using AFM by analogy in the paper [19]. On the other hand, large-scale decomposition can be used for broader tasks related to the study of technological processes that led to the final form of the studied object. For example, a large-scale decomposition of the submarine topography (Sea of Japan) was performed in the study of [20] using the method of two-dimensional singular spectrum analysis for comparing with the tectonic features of the region over a long time period to interpret the stages and scales of tectonic processes determined by the geometry and extent of the selected folded deformations.

One of the most effective methods of studying the features of the surface topography is the application of morphometric variables, widely used in the study of the Earth's surface in geomorphometry. Geomorphometry is a scientific discipline with a developed physical and mathematical theory and a powerful apparatus of computational methods,

the subject of which is mathematical modeling and analysis of topography, as well as the relationships between it and other components of geosystems [21]. The international research experience in the field of geomorphometry is summarized in a series of analytical reviews and books [21–31]. The initial data for modeling are DEMs.

A morphometric value is an unambiguous bivariate function describing the properties of a topographic surface. Each morphometric variable characterizes a certain feature of the local geometry of the surface under study, i.e. it has its own physical and mathematical meaning. Morphometric variables are calculated from the DEM using finite-difference methods or using specialized algorithms. A fairly complete list of morphometric variables, as well as calculation formulas and algorithms are given in [21,32,33].

Earlier, some of the authors of this paper considered the application of geomorphometry experience to study the shape of wafers and structures based on them [34–37], including round thin-film membranes [34]. DEMs acquired by optical profilometry [34–36] and AFM [37] were processed. This study includes the further development of this direction and the application of geomorphometric approaches to study the shape of elements of X-ray optics.

The objective of the article is to study the surface features of X-ray optics parts using morphometric variables; to determine the list of information that can be obtained with such an analysis in comparison with standard methods of analyzing topographic maps.

1. Materials and methods

The following X - ray optical elements were studied:

• spherical concave substrate with a diameter of 160 mm, with a radius of curvature of 297.4 mm, made of fused quartz of the KV grade (hereinafter referred to as „sample No. 1“) (Figs. 1–3);

• spherical concave substrate with a diameter of 66 mm, a radius of curvature of 345.4 mm, made of fused quartz of the KV grade (hereinafter referred to as „sample No. 2“) (Fig. 4).

The studied samples were made using mechanical lapping and ion-beam etching. A blank was formed using mechanical lapping with the minimum achievable deviations of the resulting shape from the calculated sphere, and then the surface shape was etched by ion-beam etching to the required parameters. Ion beam etching was carried out in two stages. The axisymmetric errors in the shape of the surface were corrected by a wide-aperture ion source through a mask at the first stage. The final correction of local errors in the shape of the surface was performed by a small-sized ion beam using a source with a focusing ion-optical system at the second stage.

Mechanical lapping was carried out on a 3PD-350 polishing and lapping machine using several types of suspensions based on an aqueous solution of cerium oxide micropowders (CeO_2) with a sequential reduction of the grit size to 20 nm. The radius of curvature was monitored using a SuperSpherotronic HR spherometer.

A wide-aperture ion source KLAN-163M was used for axisymmetric correction. An axisymmetric part was extracted from the DEM prior to processing which was used to calculate the diaphragm cutting the ion beam. The processing was carried out according to the scheme shown in Fig. 5, *b*. A shaped diaphragm was installed between the wide-aperture source of accelerated ions and the workpiece. The diaphragm cut off the ion beam in such a way that when the workpiece was rotated behind it, the material was removed from the surface of the workpiece with the required dependence of the etching depth on the radius.

Local correction was performed using the KLAN-12M ion source with an ion-optical focusing system. This source formed a beam of accelerated ions with the following parameters: the ion current density distribution in the plane of the processed sample is close to Gaussian, the width at half height $d \approx 3.3$ mm, the maximum ion current density up to 95 mA/cm^2. The processing was performed with neutralized ions Ar^0 with energy $E_{ion} = 1000$ eV.

Sample No. 2 was studied at various process stages: after processing by mechanical lapping [15] (Fig. 4, *a, d*), then after axisymmetric correction by a wide-aperture ion source (Fig. 4, *b, e*) through a special etching mask (Fig. 5, *c*), then after local correction by a small ion beam (Fig. 4, *c, f–i*) [16].

An interferometer with diffraction reference wave was used to form DEMs [17]. A specific feature of this interferometer is the use of a spherical reference wave source based on a single-mode optical fiber with a subwavelength output aperture. This instrument has a subnanometer, RMS < 1 nm, accuracy of measurements of the deviation of the surface shape of optical parts from a sphere with a numerical aperture to NA = 0.28.

Sample No. 1 was measured when it was fixed on a turntable in 12 positions (the angle of rotation between measurements $30 \pm 0.5^\circ$).

The resolution of the DEM (the size of the DEM) was reduced by linear interpolation to speed up the calculations.

For the sample No. 1, the DEM size was 1036×1036, the grid size (DEM resolution) was 0.145 mm for the case of the original (non-smoothed) DEM; the DEM size was 267×267, the grid size was 0.563 mm for the DEM after resolution reduction. The elevation difference (PV) and mean square roughness (RMS) were PV = 35.5 nm, RMS = 4.5 nm.

For the sample No. 2, the DEM size was 374×374, the grid size was 0.176 mm after processing by mechanical lapping; the DEM size was 377×377, the grid size was 0.175 mm after axisymmetric processing; the DEM size was 369×369, the grid size was 0.174 mm after local processing. PV = 137.8 nm, RMS = 18.3 nm after mechanical lapping treatment, PV = 78.5 nm, RMS = 9.9 nm after axisymmetric processing, PV = 41.2 nm, RMS = 3.8 nm after local processing. Calculations were carried out only for DEM with reduced resolution for sample No. 2.

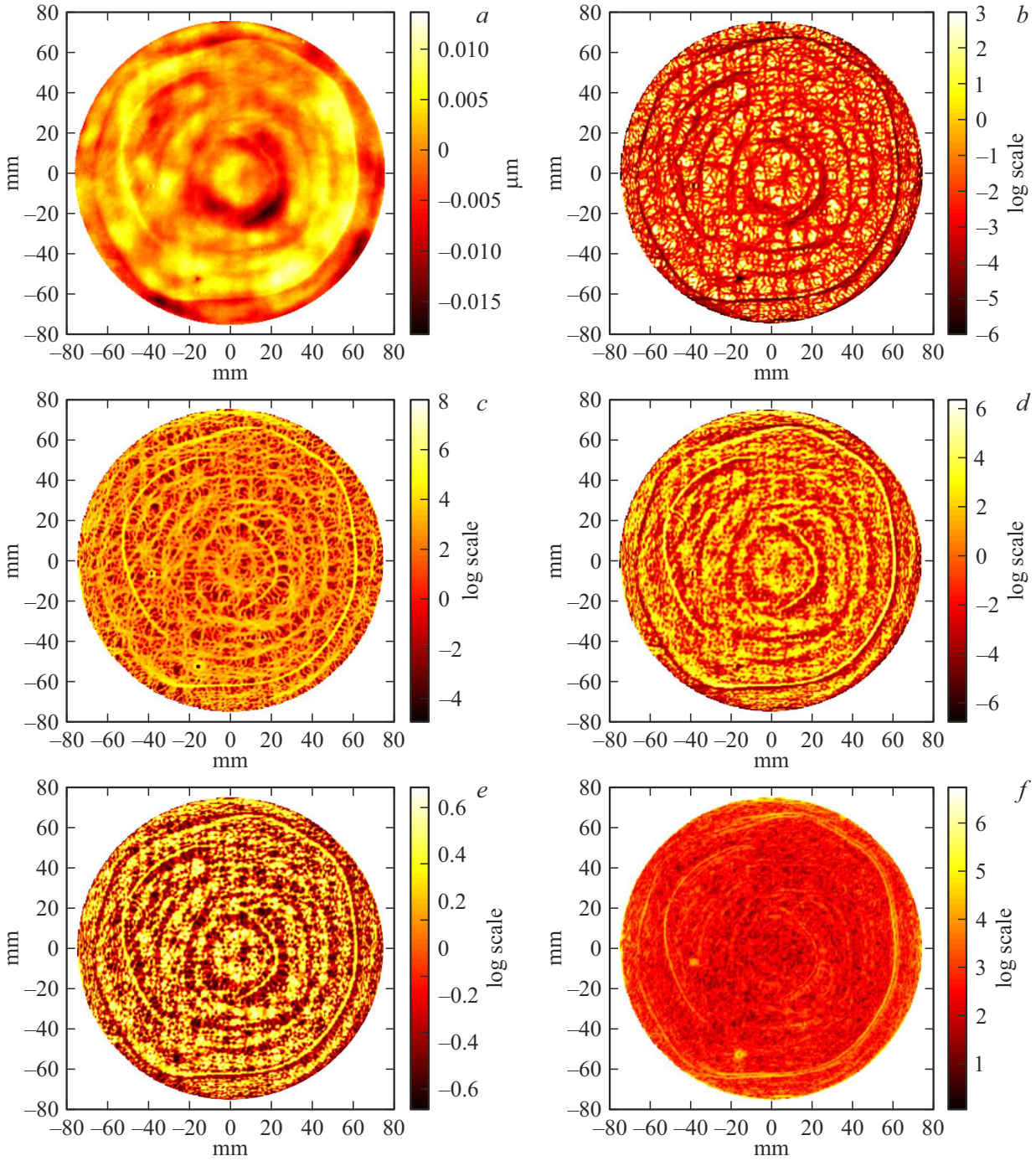

Figure 1. Sample No. 1 (spherical concave substrate): DEM (*a*) and calculated morphometric variables (*b–f*): minimum curvature $k_{\min}$ (*b*), maximum curvature $k_{\max}$ (*c*), mean curvature H (*d*), shape index ShI (*e*), unsphericity M (*f*). The number of expansion coefficients for the approximation: $n = 300$.

A universal spectral analytical method using Chebyshev polynomials of the first kind and Feyer summation was applied to calculate morphometric variables [38]. In contrast to the Zernike polynomials widely used for processing X-ray optic DEMs [39], the advantage of using which is the relationship with the main typical aberration distortions, this method preserves important topographic features when processing DEM for developers, such as ring structures and „horizontal stripes“, discussed in detail below. In addition, the method is less costly in terms of computing time. The universal spectral analytical method is designed to process regular DEMs within a single scheme, including global approximation of the DEM, generalization and noise suppression in the DEM, as well as the calculation of morphometric variables based on the analytical calculation of partial derivatives. Calculations were performed in

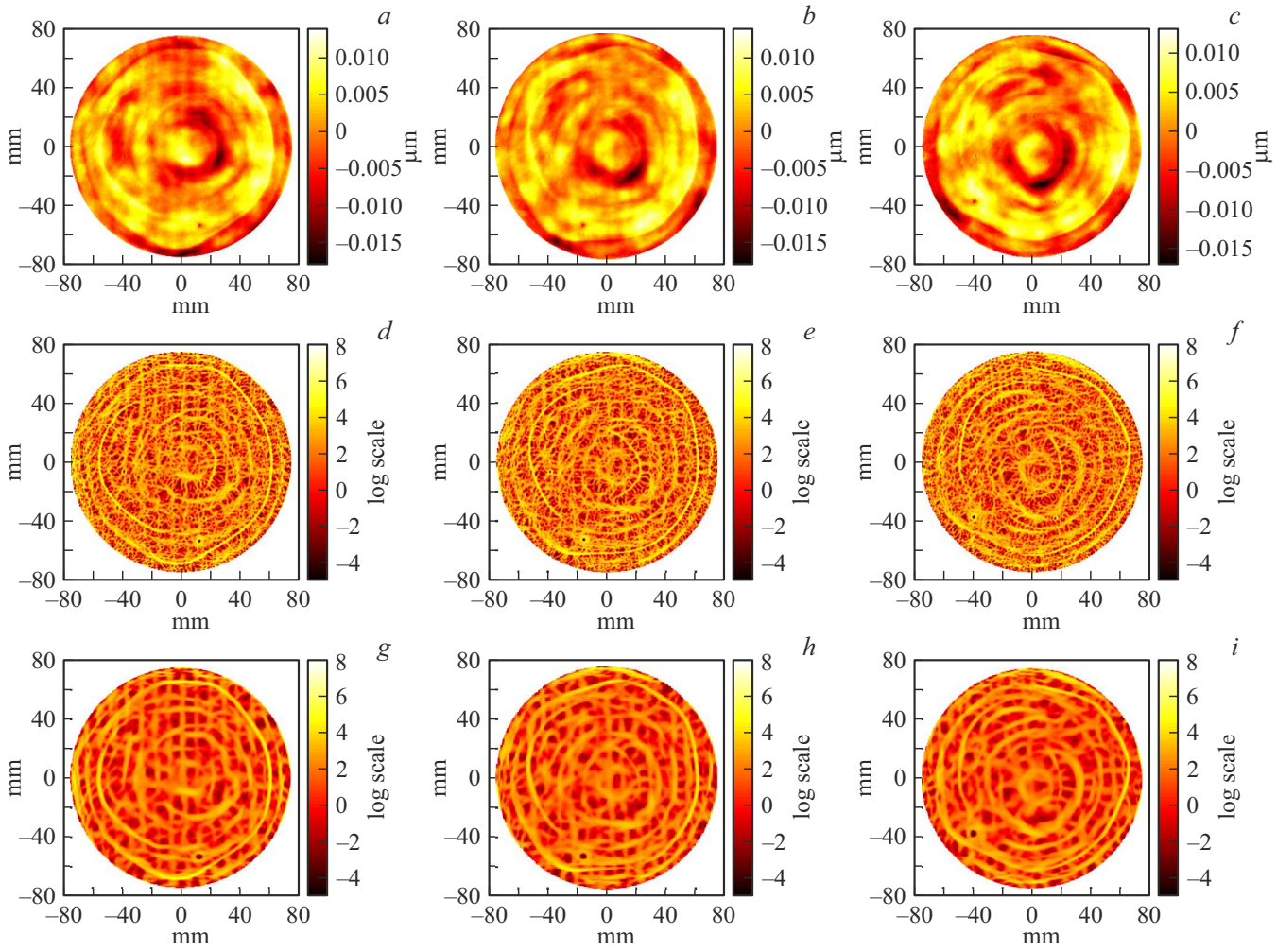

Figure 2. Sample No. 1 (spherical concave substrate): DEM (a–c) and calculated maximum curvature k_{max} (d–f): rotation angle 210° (a, d, g), 240° (b, e, h), 270° (c, f, i). The number of expansion coefficients for the approximation: $n = 300$ (d–f), $n = 100$ (g–i).

Matlab software environment using the author's program. From 100 to 600 expansion coefficients of the initial elevation function by Chebyshev polynomials were used.

Since morphometric variables are usually characterized by a wide dynamic range of values, the logarithmic scale [21,33] is used for displaying to avoid loss of information about their spatial distribution.

2. Results and discussion

Figures 1–4 shows examples of maps of calculated morphometric variables for X-ray optics objects. Each morphometric variable displays the features of the local topography of the studied objects in its own way, in accordance with its physical and mathematical sense.

Positive values of the minimum curvature k_{min} (Fig. 1, b, 3, 4 d–f, h) highlight local convex topographic elements, and its negative values indicate elongated concave topographic forms.

Positive values of maximum curvature k_{max} (Fig. 1, c, 2, 4, it g) indicate elongated convex topographic forms, and its negative values indicate local concave structures.

Mean curvature H (Fig. 1, d) determines the preferred bending direction. For convex local surface areas $H > 0$, for concave $H < 0$, for local flattening areas $H = 0$.

Unsphericity M (Fig. 1, f) shows the extent of deviation of the shape of the topographic element from the spherical shape. On the surface of the sphere, $M = 0$. Unsphericity is effectively used to evaluate defects like cracks [36,40].

The shape index ShI (Fig. 1, e) is a continuum expression of a discrete Gaussian classification of surface forms. Its positive values refer to convex topographic forms, and negative vales denotes concave forms; its absolute values from 0.5 to 1 correspond to elliptical surfaces (hills and closed depressions), and the values from 0 to 0.5 correspond to hyperbolic surfaces (saddles) [37].

The calculated data for the sample No. 1 in Fig. 1 demonstrate the applicability of morphometric variables for assessing the topographic features of X-ray optical

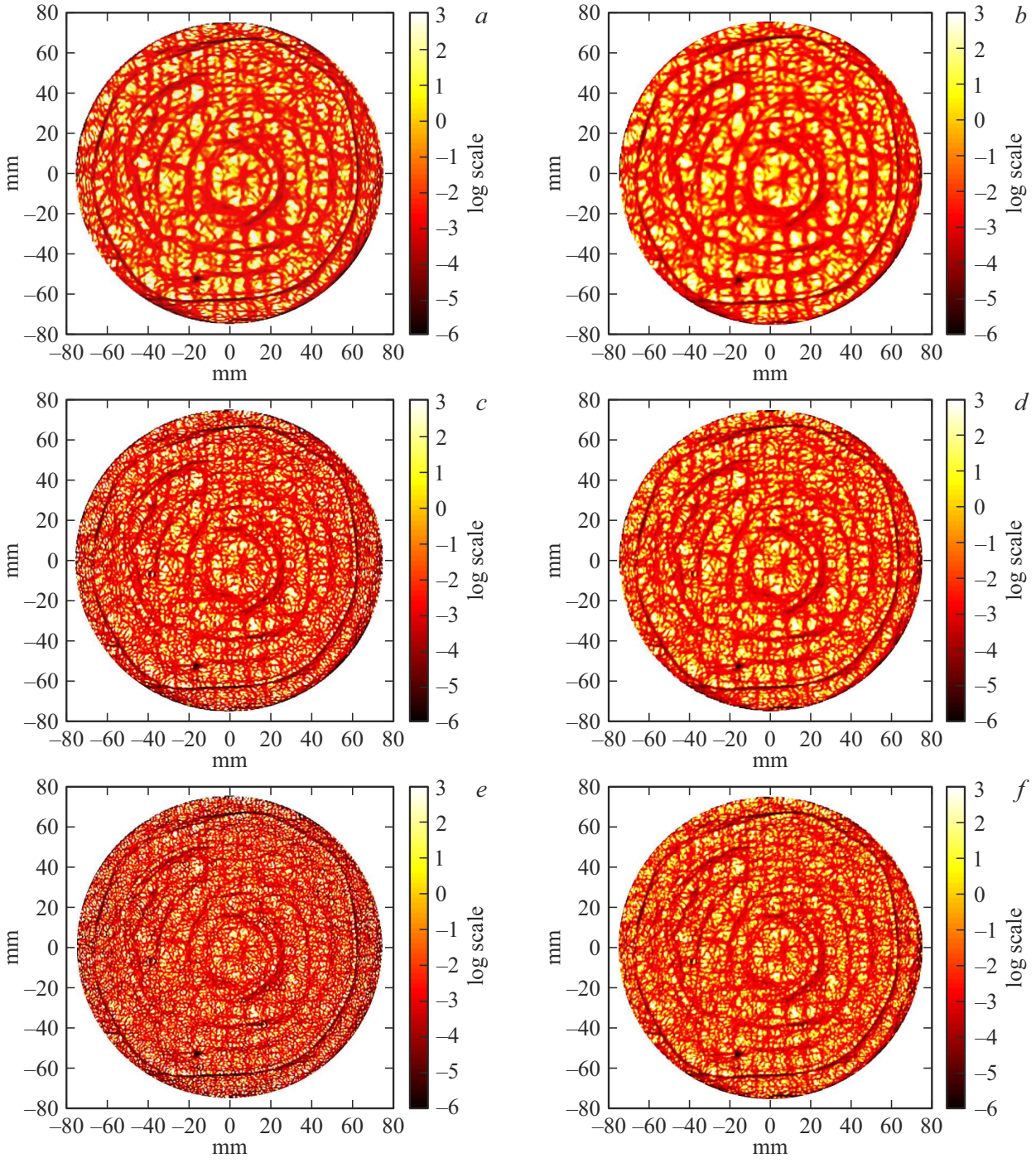

Figure 3. Calculated minimum curvature $k_{\min}$ for sample No. 1 (Fig. 1, *a*): calculation using the initial (uncoated) DEM (*a, c, e*), calculation using the smoothed DEM (the DEM after resolution reduction) (*b, d, f*). The number of expansion coefficients for the approximation: $n = 200$ (*a, b*), 300 (*c, d*), 400 (*e, f*).

elements and show the possibilities of visual detection of topographic inhomogeneities (local bumps, depressions, etc.) in accordance with the above-listed physical and mathematical sense of the morphometric variables used. For example, a small defect-pit in the lower left part of the figure corresponds to negative values of minimum curvature $k_{\min}$, maximum curvature $k_{\max}$, mean curvature H. Both this defect and, in general, the areas of the greatest topographic change are clearly visible on the unsphericity map M (the highest values of M).

Similarly, Fig. 4 shows the efficiency of using this technique for processing the DEM of the sample No. 2 at various stages of processing. It is possible to see „beams“ radiating from the center of the sample corresponding to

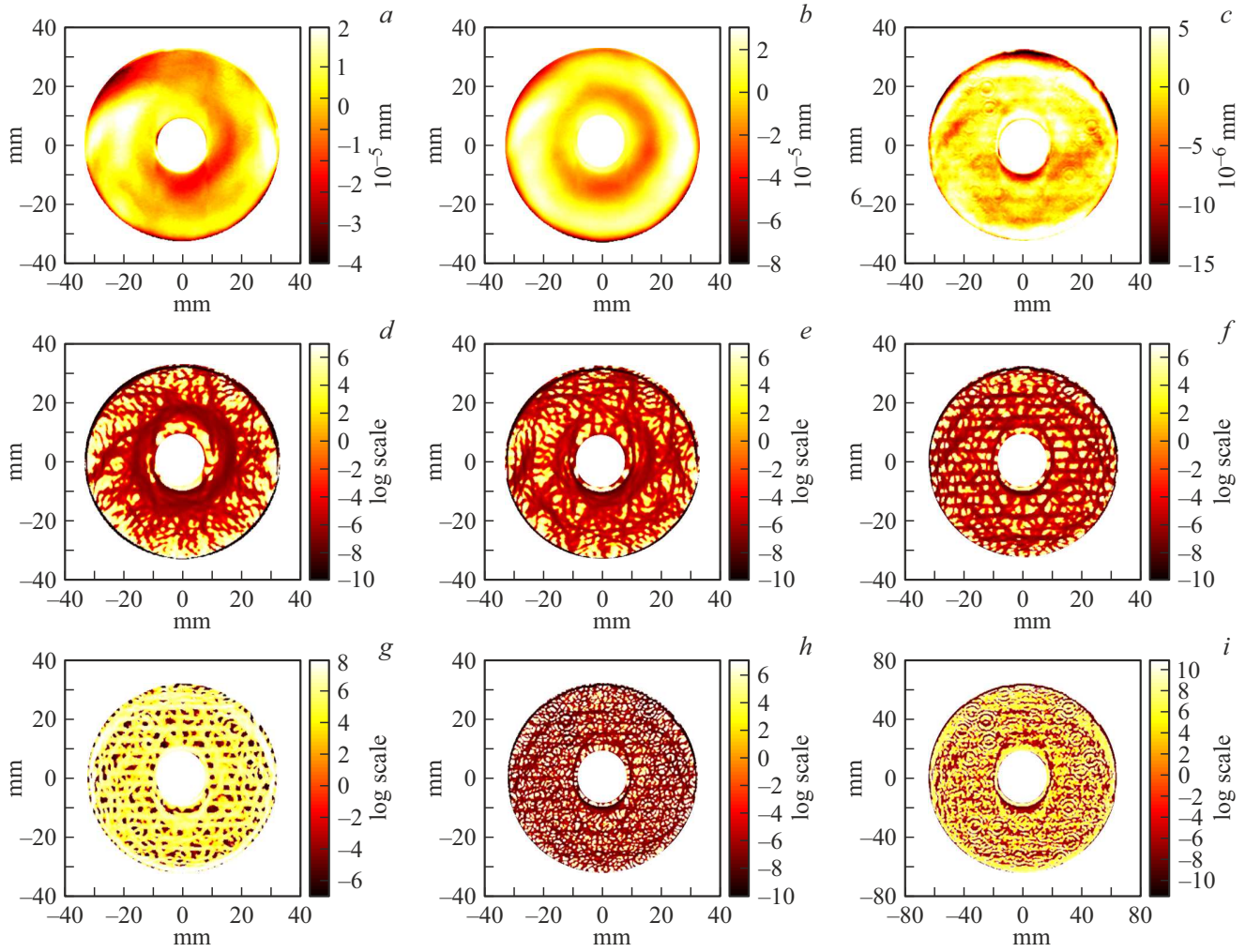

Figure 4. DEM (a–c) and calculated morphometric variables (d–i) for sample No. 2 (spherical concave substrate) at various stages of processing: after processing by the method of mechanical lapping (a, d), after axisymmetric processing (b, e), after local processing (c, f–i). Morphometric variables: $k_{\min}$ (d–f, h), $k_{\max}$ (g), H (i). The number of expansion coefficients n for the approximation: $n = 100$ (d–g), 200 (h, i).

sufficiently extended concave regions on Fig. 4, d based on the smallest values on the map of minimum curvature $k_{\min}$ which, with due experience, can be partially seen on the DEM map (Fig. 4, a; for example, the largest „beam“ is closer to the left boundary of the sample). However, it is obvious that on the $k_{\min}$ map the visualization is much more visual. The extended concave regions are also visible on the $k_{\min}$ map in Fig. 4, e (corresponding to their position in Fig. 4, b — in this case, for extended areas, you can visually trace the correlation), in addition, it is possible to analyze the location of local concave regions on extended convex areas (for example, on a massive hillock on the left side of the sample), which are on the DEM map (Fig. 4, b) not visible. However, the most interesting figure is Fig. 4, f — in this case, it can be seen that the smallest values of the minimum curvature $k_{\min}$ form „horizontal lines“. The same lines are visible on the map of maximum curvature $k_{\max}$ (Fig. 4, g). However, it is almost impossible to determine their presence on the DEM map (Fig. 4, c).

In general, important features of the topography, necessary to determine the required parameters of the technological process at the initial stages, can be evaluated directly from the DEM (Fig. 1, a) without resorting to the capabilities of geomorphometry due to the rather large extent of the irregularities of the topography of the sample No. 1 (Fig. 1, a). Indeed, the maps in Fig. 1, b–f demonstrate a large number of smaller topographic inhomogeneities that are not visible against the background of the overall shape of the DEM structure, but they are not so important at the current stage of processing. By analogy, the DEM in Fig. 4, a was used mainly to isolate the axisymmetric component in order to calculate the required mask for etching (Fig. 5).

However, all remaining inconsistencies already become important closer to the completion of the technological treatments of the substrates and their achievement of the required shape. In this case, for example, knowing the position of local bumps, they can be taken into account

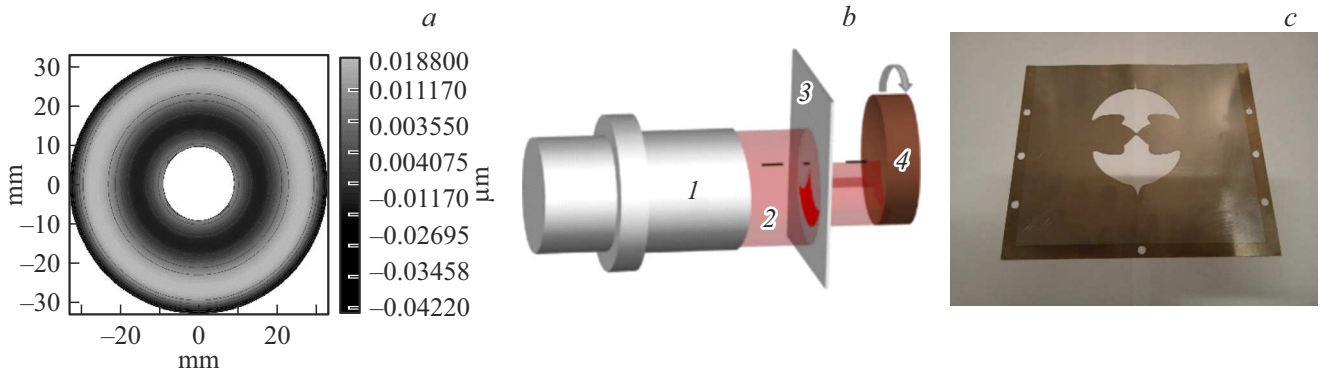

Figure 5. Axisymmetric part of the surface map (*a*); scheme of the experiment of axisymmetric surface treatment: *1* — wide-aperture ion source, *2* — quasi-parallel ion beam, *3* — shaped diaphragm, *4* — workpiece (*b*); mask for axisymmetric processing (*c*).

when developing a procedure for local etching of this sample and subsequently achieve greater surface evenness. In this case, an example of calculated maps of morphometric variables for the sample No. 2 after local processing is quite illustrative (Fig. 4,*f, g*), which show atypical features of the topography, such as „horizontal stripes“, unnoticeable on the DEM (Fig. 4, *c*).

It is important to note that, since a universal spectral analytical method was used for calculations, before calculating morphometric variables, the DEM approximation is carried out using Chebyshev polynomials of the first kind. The location and dimensions of the topographic patterns displayed on morphometric maps differ significantly depending on the depth of expansion of the original DEM used (i.e., on the number of expansion coefficients n used in the reconstruction of the approximated DEM). The smaller the n value, the stronger the degree of generalization (smoothing) of the DEM. Therefore, the use of a different number of polynomials for approximation makes it possible to identify topographic patterns related to different levels of the spatial hierarchy (scale). In fact, this is conducting a multi-scale analysis similar to the methods described in [18–20]. This leads to the fact that in practice, when studying structure DEM, it is necessary to use a different number of polynomials to identify various features of the surface topography. In particular, at $n = 200$, due to the greater detail of the image (Fig. 4, *h*), „horizontal stripes“ become almost unnoticeable (compared to the case of $n = 100$, Fig. 4,*f*). However, a series of concentric circles is well visualized on the maps from Fig. 4, *h, i* at $n = 200$, which merge with the general picture in Fig. 4,*f* at $n = 100$.

These ring structures are an artifact of measurements and are caused by the presence of dust particles on the recording system of the interferometer. It is possible to see that their location on different maps is the same. For example, the circle located in the middle between the center of the sample and its left edge is most clearly visible for the sample No. 1 in Fig. 2, which on the maps of maximum curvature $k_{\max}$ (Fig. 4, *d–f*) corresponds to its small values. The position of this defect does not change when the sample is rotated (Fig. 2). At the same time, the position of another small defect that was discussed earlier (a small defect is a pit in the lower left part of Fig. 2, *b*) changes accordingly to what is expected (Fig. 2). With a decrease in the degree of smoothing (an increase in the degree of polynomials n), ring structures become more clearly visualized (Fig. 3, *e*).

Continuing the discussion of the features of conducting multi-scale analysis and artifacts in the DEM, it is worth noting that the experimentally processed DEMs of real structures include:

1) information about the studied samples;

2) relatively constant errors and artifacts caused by the recording system (dust particles, etc.);

3) variable errors and artifacts caused by inhomogeneity of the medium (air flows, vibrations, etc.).

This leads to the fact that the DEM maps themselves for the same sample are not identical for different measurements (for example, the DEM in Fig. 2 do not perfectly correspond to the models rotated by an angle 30°). Therefore, when analyzing topographic inhomogeneities using morphometric variables, it should be remembered that the results obtained can be both indicators of the characteristics of the sample under study and the consequence of introduced errors, including random (not systematic) ones. In the case of studying X-ray optics objects with DEM with a elevation difference of about a hundred nanometers or less, this effect manifests itself at various levels of the spatial hierarchy (Fig. 2).

This means that in general there is no need to use the original (non-smoothed) DEM maps for calculations instead of more convenient from the point of view of the time of computing of smoothed DEM. Fig. 3 shows the results of calculating the minimum curvature $k_{\min}$ of the sample No. 1 for the initial and smoothed DEM. It can be seen that for $n = 200$, the calculated $k_{\min}$ maps are practically indistinguishable (Fig. 3, *a, b*). Naturally, the situation is similar with a smaller degree of the polynomial n. The level of detail increases with an increase of the degree of the polynomial n and it is already possible to see the differences

(Fig. 3, *c, d*) with $n = 300$ and starting with $n = 400$ they already become very noticeable (Fig. 3, *e, f*).

Concluding this section, it is worth noting that, in addition to the morphometric variables described, the following parameters were also calculated and analyzed: Gaussian curvature, difference curvature, Laplacian, curve dness, catchment area, dispersive area, topographic index, etc. (LandLord 4.0 program was used for the latter three [41]). It was found that the ring structures are most clearly visualized on the maps of the topographic index; otherwise, the results repeat those obtained in Matlab.

Conclusion

An approach to the study of the surface topographic features of X-ray optical elements based on the use of morphometric variables is proposed. The approach was tested on two spherical concave substrates: diameter 66 mm and radius of curvature 345.4 mm, diameter 160 mm and radius of curvature 297.4 mm.

It was demonstrated that these approaches are useful for the following tasks:

- a more clear visualization of topographic inhomogeneities (local bumps, depressions, etc.), which potentially becomes most relevant closer to the completion of processing stages;
- detection of „fine“ topographic inhomogeneities that are not displayed on the maps of the original DEM, in particular, „horizontal stripes“ were detected on the maps of curvatures;
- visualization of measurement artifacts (for their subsequent elimination from the DEM), in particular, ring structures caused by the presence of dust particles on the recording system of the interferometer were clearly manifested.

The provided information is necessary for the developers of X-ray optical elements to control the supplied technological operations and processes in order to achieve the required shape of the parts.

Also, summarizing the conducted studies, it can be concluded that it is necessary to carry out several measurements of the same sample to assess the topographic features of X-ray optics objects. This is necessary for:

1) confirmation that the observed topographic features are not the result of random errors;

2) determination of systematic errors (for example, artifacts like ring structures) and their removal from the DEM under study.

Funding

The study was supported by the Russian Science Foundation, project No. 22-21-00614. The equipment of the R&D Center „MEMSEC“ (MIET) was used.

Conflict of interest

The authors declare that they have no conflict of interest.

References

[1] A.A. Akhsakhalyan, A.D. Akhsakhalyan, D.G. Volgunov, M.V. Zorina, M.N. Toropov, N.I. Chkhalo. Poverkhnost'. Rentgenovskie, sinkhrotronnye i neytronnye issledovaniya **7**, 93 (2015) (in Russian). DOI: 10.7868/S0207352815070033

[2] E.B. Klyuenkov, V.N. Polkovnikov, N.N. Salashchenko, N.I. Chkhalo. Bull. Russ. Academ. Sci.: Phys., **72** (2), 188 (2008).

[3] V.V. Gribkov, A.S. Markelov, V.N. Trushin, E.V. Chuprunov. Pribory i tekhnika eksperimenta, **1**, 136 (2018) (in Russian). DOI: 10.7868/S0032816218010196 [V.V. Gribko, A.S. Markelov, V.N. Trushin, E.V. Chuprunov. Instruments and Experimental Techniques, **61** (1), 148 (2018). DOI: 10.1134/S0020441218010165]

[4] A.A. Akhsakhalyan, A.D. Akhsakhalyan, S.A. Garakhin, N.N. Salashchenko, M.N. Toropov, N.I. Chkhalo, N.F. Erkhova, A.S. Kirichenko, S.V. Kuzin. Tech. Phys., **64** (11), 1680 (2019). DOI: 10.1134/S1063784219110033

[5] A. Khudolei, G. Gorodkin, L. Gleb, A. Alexandronets. Nauka i innovatsii, **6** (148), 20 (2015) (in Russian).

[6] D.G. Denisov, O.S. Ageeva. Kontenant, **19** (4), 10 (2020) (in Russian).

[7] A.P. Semenov, A.N. Ignatov, A.B. Nikonov, V.E. Patrikeev, A.B. Morozov, A.Yu. Papaev, M.A. Laukhin, V.N. Pyshnov, A.O. Lyakhovets, E.S. Golubev, A.V. Smirnov. Kontenant, **20** (3), 7 (2021) (in Russian).

[8] A.P. Semenov, M.A. Abdulkadyrov, N.S. Dobrikov, A.N. Ignatov, V.E. Patrikeev, A.Yu. Papaev, A.V. Polyanshchikov, V.V. Pridnya. J. Opt. Technol., **84** (11), 767 (2017). DOI: 10.1364/JOT.84.000767

[9] N.I. Chkhalo, N.N. Salashchenko. Bulletin of the Russian Academ. Sci.: Phys., 83 (2), 105 (2019). DOI: 10.3103/S1062873819020072

[10] V.V. Gribko, A.S. Markelov, V.N. Trushin, E.V. Chuprunov. J. Surf. Investigation: X-Ray, Synchrotron and Neutron Techniques, **11** (3), 505 (2017). DOI: 10.1134/S1027451017030077

[11] V.V. Gribko, A.S. Markelov, V.N. Trushin, E.V. Chuprunov. Instruments and Experimental Techniques, **62** (5), 703 (2019). DOI: 10.1134/S0020441219040183

[12] N.N. Salashchenko, M.N. Toporov, N.I. Chkhalo. Bull. Russ. Academ. Sci.: Phys., **74** (1), 53 (2010). DOI: 10.3103/S1062873810010144

[13] A.K. Chernyshev, I.V. Malyshev, A.E. Pestov, N.I. Chkhalo. Tech. Phys., **64** (11), 1560 (2019). DOI: 10.1134/S1063784219110069

[14] M.V. Zorina, I.M. Nefedov, A.E. Pestov, N.N. Salashchenko, S.A. Churin, N.I. Chkhalo. J. Surfa. Investigation: X-Ray, Synchrotron and Neutron Techniques, **9** (4), 765 (2015). DOI: 10.1134/S1027451015040394

[15] M.N. Toropov, A.A. Akhsakhalyan, M.V. Zorina, N.N. Salashchenko, N.I. Chkhalo, Yu.M. Tokunov. Tech. Phys., **65** (11), 1873 (2020). DOI: 10.1134/S1063784220110262

[16] A. Chernyshev, N. Chkhalo, I. Malyshev, M. Mikhailenko, A. Pestov, R. Pleshkov, R. Smertin, M. Svechnikov, M. Toropov. Precis. Eng., **69**, 29 (2021). DOI: 10.1016/j.precisioneng.2021.01.006

[17] A.A. Akhsakhalyan, N.I. Chkhalo, N. Kumar, I.V. Malyshev, A.E. Pestov, N.N. Salashchenko, M.N. Toropov, B.A. Ulasevich, S.V. Kuzin. Precis. Eng., **72**, 330 (2021). DOI: 10.1016/j.precisioneng.2021.05.011
[18] O.K. Garishin, R.I. Izyumov, A.L. Svistkov. Vestnik Permskogo un-ta. Fizika, **1** (39), 36 (2018) (in Russian). DOI: 10.17072/1994-3598-2018-1-36-45
[19] N.I. Uzhegova, A.L. Svistkov. Computational Continuum Mechanics, **9** (3), 366 (2016) (in Russian). DOI: 10.7242/1999-6691/2016.9.3.30
[20] R.A. Korotchenko, A.N. Samchenko, I.O. Yaroshchuk. Oceanology, **54** (4), 497 (2014). DOI: 10.1134/S0001437014030047
[21] I.V. Florinsky. *Digital Terrain Analysis in Soil Science and Geology*. 2-nd ed. (Elsevier Academic Press, Amsterdam, 2016)
[22] Y. Deng. Progress in Physical Geography, **31** (4), 405 (2007). DOI: 10.1177/0309133307081291
[23] T. Hengl, H.I. Reuter (eds.) *Geomorphometry: Concepts, Software, Applications* (Elsevier, Amsterdam, 2009)
[24] Z. Li, Q. Zhu, C. Gold. *Digital Terrain Modeling: Principles and Methodology* (CRC Press NY., 2005)
[25] G. Lv, L. Xiong, M. Chen, G. Tang, Y. Sheng, X. Liu, Z. Song, Y. Lu, Z. Yu, K. Zhang, M. Wang. J. Geograph. Scie., **27** (11), 1389 (2017). DOI: 10.1007/s11442-017-1442-0
[26] J. Minár, J. Krcho, I.S. Evans. *Reference Module in Earth Systems and Environmental Sciences* (2016), DOI: 10.1016/B978-0-12-409548-9.10260-X
[27] I.D. Moore, R.B. Grayson, A.R. Ladson. Hydrological Processes, **5** (1), 3 (1991). DOI: 10.1002/hyp.3360050103
[28] R.J. Pike. Progr. Phys. Geogr., **24** (1), 1 (2000). DOI: 10.1177/030913330002400101
[29] J.P. Wilson. Geomorphology, **137** (1), 107 (2012). DOI: j.geomorph.2011.03.012
[30] J.P. Wilson *Environmental Applications of Digital Terrain Modeling* (Wiley-Blackwell Chichester, 2018)
[31] J.P. Wilson, J.C. Gallant (eds.) *Terrain Analysis: Principles and Applications* (Wiley NY., 2000)
[32] P.A. Shary. Mathem. Geology, **27** (3), 373 (1995). DOI: 10.1007/BF02084608
[33] P.A. Shary, L.S. Sharaya, A.V. Mitusov. Geoderma, **107** (1/2), 1 (2002). DOI: 10.1016/S0016-7061(01)00136-7
[34] A.A. Dedkova, I.V. Florinsky, N.A. Djuzhev. Phys. Usp., **65**, 706 (2022). DOI: 10.3367/UFNe.2021.10.039076
[35] A.A. Dedkova, I.V. Florinsky, N.A. Djuzhev. Tech. Phys., **67** (8), 933 (2022). DOI: 10.21883/TP.2022.08.54553.101-22
[36] A.A. Dedkova, E.E. Gusev, N.A. Dyuzhev, M.Y. Fomichev, M.Y. Shtern, I.V. Florinsky. Russ. J. Nondestructive Testing, 57 (11), 1000 (2021). DOI: 10.1134/S1061830921110073
[37] A.A. Dedkova, I.V. Florinsky. V sb.: *Matematicheskaya biologia i bioinformatika*. Doklady IX Mezhdunarodnoy konferentsii (Pushchino, 2022), 231 p, DOI: 10.17537/icmbb22.26
[38] I.V. Florinsky, A.N. Pankratov. Intern. J. Geograph. Inform. Sci., **30** (12), 2506 (2016). DOI: 10.1080/13658816.2016.1188932
[39] V. Lakshminarayanan, A. Fleck. J. Modern Optics, **58** (7), 545 (2011). DOI: 10.1080/09500340.2011.554896
[40] M. Foroutan, S.J. Marshall, B. Menounos. J. Glaciology, **65** (254), 971 (2019). DOI: 10.1017/jog.2019.71
[41] Electronic source. Available at: http://iflorinsky.impb.ru/ll-ru.htm

Translated by A.Akhtyamov